https://doi.org/10.48048/tis.2025.8985

The Effect of Mixed Lipid Concentrations and Sucrose on the Size of the Lipid Nanoparticles Containing mRNAs

Wahyu Widayat[1,2,3], Ari Hardianto[1,4,*], Rahma Ayu Hidayati[4], Neni Nurainy[5] Muhammad Burhanudin[4], Muhammad Yusuf[3,4] and Toto Subroto[3,4]

[1]Molecular Biotechnology and Bioinformatics Research Center, Universitas Padjadjaran, West Java 40133, Indonesia
[2]Faculty of Pharmacy, Universitas Mulawarman, East Kalimantan 75119, Indonesia
[3]Doctoral Program in Biotechnology, Graduate School, Universitas Padjadjaran, West Java 40132, Indonesia
[4]Department of Chemistry, Faculty of Mathematics and Natural Sciences, Universitas Padjadjaran, West Java 45363, Indonesia
[5]PT Bio Farma, West Java40161, Indonesia

([*]Corresponding author's e-mail: a.hardianto@unpad.ac.id)

Received: 10 September 2024, Revised: 18 September 2024, Accepted: 25 September 2024, Published: 10 November 2024

Abstract

The development of messenger RNA (mRNA) vaccines has been transformed using lipid nanoparticles (LNPs) as delivery systems. This study evaluates the impact of lipid mixture molar concentration and the addition of sucrose as a cryoprotectant on the size and stability of LNPs encapsulating mRNA. Using a microfluidic mixing technique, we formulated LNPs with varying lipid concentrations and analyzed their size, size distribution, and encapsulation efficiency through dynamic light scattering and a RiboGreen assay. Results indicated that higher lipid concentrations not only improved encapsulation efficiency but also maintained LNPs within the ideal size range of 80-120 nm, crucial for optimal biodistribution and immune cell uptake. Furthermore, the addition of sucrose significantly stabilized the LNPs against size changes during freeze-thaw cycles, particularly at lower temperatures. This study underscores the importance of optimizing lipid and sucrose concentrations to enhance the stability and functionality of LNPs, providing insights that could enhance the efficacy and storage stability of mRNA vaccines.

Keywords: Lipid nanoparticles (LNPs), Microfluidic, Sucrose, Mixed lipid molar concentration, Size stability

Introduction

In December 2020, history was made in vaccinology, mRNA vaccines from pharmaceutical companies Moderna (SpikeVax) and Pfizer-BioNTech (Comirnaty) received Emergency Use Authorization (EUA) during the COVID-19 pandemic with a protection rate of 95% [1-3]. LNPs are a crucial technology in delivering mRNA-based therapies, offering protection and efficient delivery into target cells [4]. The importance of LNPs in mRNA delivery lies in their ability to overcome various biological barriers, including cell membranes and degradation by nucleases [5], thus enabling the safe and effective delivery of therapeutic mRNA molecules [6-8].

LNPs are a next-generation delivery system derived from liposomes [9], classified as small unilamellar vesicles. LNPs consist of 4 lipid components: Ionizable lipids, phospholipids, sterol lipids, and PEG2000-DMG [10,11]. Ionizable lipids are the key to the successful encapsulation of RNA within LNPs [12,13]. These lipids are specifically designed to carry a positive charge, enabling them to bind to the negatively charged mRNA and become neutral in physiological solutions (pH 7.4) within the body [5,14].

Lipid-based delivery systems, first developed by Alec Bangham to mimic the structure of bilayer lipid membranes [15]. The term LNP-mRNA synthesis refers

to the process of encapsulating mRNA within LNPs [16], while nanoprecipitation is the mixing of a substance (lipid) in an organic solvent phase with a substance in an aqueous phase to produce nanoparticles [17]. Microfluidics is a method used to formulate LNP-mRNA [18] that adapts the nanoprecipitation process [19]. The microfluidic device consists of a chaotic mixing chip [20]. This chip has 2 channels that bring the lipid and mRNA phases together at specific velocities, allowing for the self-assembly process (nucleation and growth) [21,22], which occurs in a mixing channel less than 1 micrometer in size [23,24].

The efficacy profile of LNP-mRNA is influenced by its physical parameters, particularly size [25]. Theoretically, LNPs of specific sizes can affect cellular uptake, biodistribution, and immunogenicity [26]. Typically, LNP-mRNA is administered intramuscularly [27], with an ideal size range of 50-200 nm [28,29] to be recognized and processed by APCs (macrophages, monocytes, and dendritic cells) before moving to the lymphatic system [30,31]. The size of LNPs is not determined by the mRNA load but by the lipid composition [32]. However, the impact of lipid mixture molar concentrations on particle size has not yet been studied in detail.

The stability of LNP-mRNA is maintained by the addition of cryoprotectant agents, which play a crucial role in reducing the damaging effects of freezing-induced stress on LNPs, thereby preserving their structural integrity and functionality during distribution. The addition of monosaccharides such as sucrose has been shown to maintain the size of LNP-mRNA [33,34], but whether sucrose also leads to an increase in size is still unknown.

Given the critical role of LNP size in therapeutic efficacy, this study aims to analyze how varying lipid molar concentrations and the addition of sucrose affect LNP-mRNA size. We also investigate size changes after buffer exchange that contribute to optimizing LNP formulations for effective mRNA delivery. Understanding these factors will optimize LNP formulations, improving mRNA delivery for therapeutic applications.

Materials and methods

Material

mRNA eGFP was purchased from Messenger bio, Citrate acid, sodium citrate, sodium chloride and etanol 96% were obtained from Merck. Phosphate buffer saline (PBS), Sucrose, Triton X-100 were obtained Sigma Aldrich. SM-102 (heptadecan-9-yl 8-((2-hydroxyethyl) (6-oxo-6-(undecyloxy) hexyl) amino) octanoate), DSPC(1,2-Distearoyl-sn-glycero-3 phosphocholine), PEG2000-DMG 1-monomethoxypolyethyleneglycol-2,3 dimyristylglycerol with polyethylene glycol of average molecular weight 2300) were obtained from Xiamen Sinopeg Biotech. Cholesterol was obtained from Nippon FINE Chemical. Nuclease free water (NFW) was obtained from Himedia dan Kit Quantit RiboGreen was obtained from Thermo.

Experimental design of molar concentrations of mixed lipid formulas

The molar concentration of the mixture lipids varied from 10 to 1000 dilution from the highest concentration 10 mM.

Tabel 1 concentration variation of mixed lipid formulas.

Lipid Mix Concentration mM	Ionizable lipid (SM-102) mM	Helper Lipid (DSPC) mM	Kolesterol mM	PEG 2000-DMG mM	mRNA concentration ug/mL
10	5	1	3.85	1.5	1.5
1	0.5	0.1	0.385	0.015	1.5
0.1	0.05	0.01	0.0385	0.0015	0.15
0.01	0.005	0.001	0.00385	0.00015	0.015

The concentration of mRNA at each lipid mixture concentration results from converting moles of eGFP mRNA to ug/mL by calculating the ratio of nitrogen to phosphate (N/P).

LNP-mRNA Formulation

The LNP-mRNA formulation was carried out by microfluidic mixing technique of ethanol and aqueous phase on a staggered herringbone chip (SHM) using a syringe pump new era model NE300. In the experiment, we use Channel A on the chip Fluidic 1460 with a channel depth of 600 μm and 8 cycle grooves. Formula composition adapted SpikeVax (Moderna) COVID-19 vaccine SM-102/DSPC/Cholesterol/PEG-DMG with a% molar ratio of 50:10:38, 5:1, 5.

Microfluidic mixing was performed at a nitrogen-to-phosphate (N/P) molar ratio of 36, a flow rate ratio (FFR) of 3:1 aqueous phase (mRNA) to ethanol phase (lipids), and a total flow rate (TFR) of 4 mL/min adapted from Bailey-Hytholt *et al*. [38]. The concentration of eGFP mRNA was calculated using the mole ratio of ionized lipid to mRNA at N/P 36.

mRNA was dissolved in 5 mM citrate buffer (pH 7.4), and each lipid was dissolved in absolute ethanol with a concentration of 10 mM and mixed according to the molar concentration in the experiment design. LNP-mRNA were collected in 4 parts of PBS pH 7.4 and concentrated (filtration) using amicon 100 kDa MCWO and washed again with PBS + sucrose pH 7.4 using a centrifuge at 1200G for 15-20 min in stages until the volume was 1 mL.

Storage of LNP-mRNA at various temperatures and cryoprotectant concentrations

LNP-mRNA eGFP was formulated as described. Then, the buffer was exchanged with PBS pH 7.4, PBS + 5% sucrose, and 10% w/v. Next, LNP-mRNA eGFP was stored at room temperature, 4 and −20°C, respectively. All samples were treated with freeze-thawing for 3 cycles at room temperature and then analyzed for particle size (d.nm) and polydispersity index (PdI) of LNP-mRNA eGFP.

Characterization LNP-mRNA

The LNP-mRNA (nm) particle size was analyzed using Malvern Zetasizer (Malvern Instrument Ltd, UK). Measurements were carried out before and after buffer exchange for each formula. In addition, measurements were also taken during storage stability testing at room temperature, 2-8 and −2°C. Measurement of particle size distribution on LNP-mRNA before concentrating directly on 500 uL volume, while after concentrating dilute 10-20 uL of LNP-mRNA in 500 uL PBS. The measurement process used a semi-micro cuvet with 2 replications.

Encapsulation efficiency of LNP-mRNA

Thaw the RiboGreen dye reagent at room temperature and away from light and the RNA standard at 4°C. Prepare 1X TE buffer (Tris-EDTA) and triton X-100 buffer (2%) in 1X TE buffer with RNAse-free water. In row A, we diluted the LNP-mRNA eGFP formula as much as 100 uL in 100 uL of TE 1X. Each row B - C was filled with 50 uL of TE 1X buffer, and D-E was filled with 50 uL of Triton 2%. Then, LNP-mRNA eGFP from row A was as much as 50 μL while rows F - G were filled with standard RNA. The standard RNA concentrations used were 2, 1, 0.5, 0.25, 0.1, and 0.05 ug/mL from a 20 ug/mL stock using TE 1X buffer and 50 μL Triton 2% added. Incubate for 10 min at 37°C, then leave at room temperature for 5 min. Add 100 μL of RiboGreen reagent to the wells that have been diluted 1:100 according to the number of wells used and homogenized. Avoid the formation of bubbles during mixing, and if there are bubbles, pop them with a needle. Measure the fluorescence at λ ex 485 nm and λ em 528 nm. Standard concentrations of RNA and mRNA eGFP were calculated using the linear regression and%EE was calculated using the formula:

$$\%EE = (1-(\text{Unencapsulated mRNA } ((\mu g)/mL))/(\text{Total mRNA } (ug/mL)))\times 100 \quad (1)$$

Results and discussion

The size (diameter) and size distribution of LNP particles become one of the important parameters in the delivery of mRNA as a vaccine [25,35]. Stability, encapsulation efficiency, drug release profile, biodistribution, and cellular uptake are some of the most affected and influenced delivery parameters by its size. The size variation of LNPs is very diverse, generally ranging from 50-500 nm and recognized by immune cells (APCs) for the endocytosis process and located in the lymph gland channel. Endocytosis of LNP-mRNA by APC cells sized 100 nm is comparable to the size of viruses, which range at 80 nm (influenza), 100 nm (SARS-CoV-2), and 120 nm (reovirus). Ionized lipids, phospholipids, cholesterol, and PEG-lipid are the

components of the lipid mixture making up the LNP structure approved by the FDA [25].

The Polydispersity Index (PdI) describes the non-uniformity of the population is a dimensionless parameter, defined as the square of the standard deviation/average value of the LNP population. The PdI value range varies from 0 (homogeneous), and 1 (heterogeneous), generally PdI ≤ 0.3 indicates a homogeneous particle population and is thus used for LNP characterization. Microfluidic mixing allows for an optimal PdI in the LNP-mRNA formulation, which is about 0.1.

In addition to the selection of lipids and the partial ratio of each lipid, the nanoparticle concentration greatly affects the final outcome of the LNP. In practice, the formation of LNPs is expensive, so the minimal concentration that can produce the targeted size and size distribution is important to be further known.

Effect each molar lipid mix concentration on distribution size LNP-mRNA

The formation of LNP is influenced by many variables, including molar ratio composition, TFR, FRR, herringbone cycle (groove), and N/P ratio [36]. We tested lipid mixture concentrations with ratios of 50:10:38.5 and 1.5 to study whether the diameter size of LNP encapsulating mRNA is affected. Several studies use a lipid mixture formula concentration (total of each lipid ratio) of 10 mM as the standard in LNP-mRNA formulation [37]. Due to limitations in providing the amount of mRNA, in the formulation, the lipid concentrations of 1 and 10 mM used the same mRNA concentration, which was 1.5 µg/mL, while for the concentrations of 0.1 and 0.01 mM, the mRNA concentrations were adjusted according to the calculation formula [38].

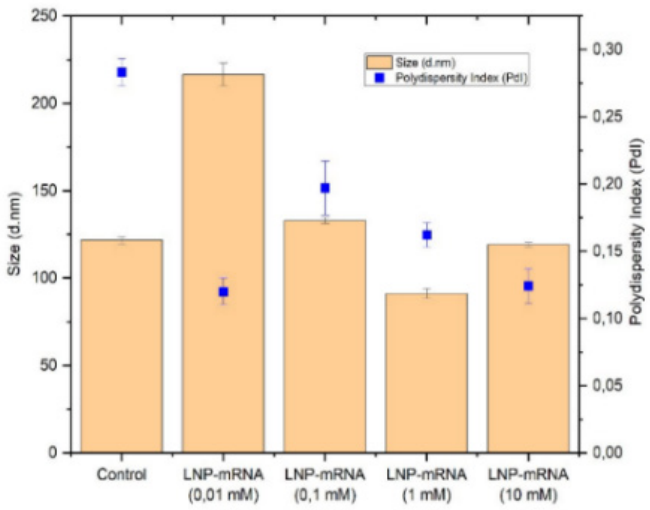

Figure 1 LNP-mRNA diameter size and PdI.

The formulation was carried out using microfluidic mixing with parameters of N/P 36, FRR 3:1 (Water: Ethanol), and TFR 4 mL/min [38] DLS analysis and PdI (**Figure 1**) show that the average diameter size of LNP from each lipid mixture concentration falls within the LNP size range. All PdI are below ≤ 0.3, indicating that the LNP-mRNA falls into the category of monodispersity. Concentrations of 0.1 and 0.01 mM produced LNP-mRNA diameters of 132.90 ± 1.66 and 216.53 ± 6.54, respectively, while 10 and 1 mM concentrations resulted in LNP-mRNA diameters within the preferred range, which are 119.23 ± 1.35 and 91.21 ± 2.79, respectively.

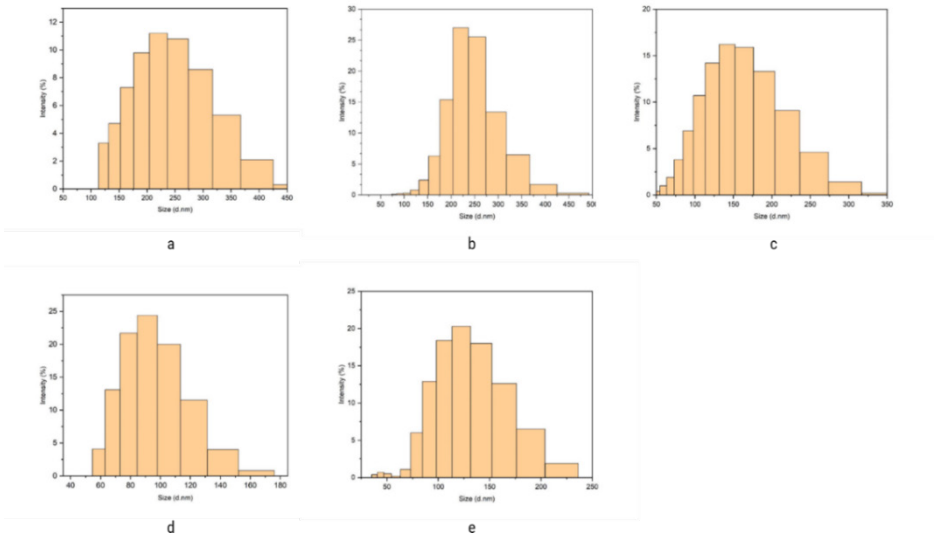

Figure 2 Intensity (%) of particle size distribution of LNP-mRNA formulated with different lipid mixture concentrations: (a) 1 mM empty mRNA (control), (b) 0.01 mM, (c) 0.1 mM, (d) 1 mM, and (e) 10 mM.

The intensity or frequency (%) of particle size distribution variation for LNP-mRNA (**Figure 2**) from each lipid mixture concentration under constant formulation variables. The particle size distribution shows a peak intensity in the 150-250 nm range, with the highest peak around 200 nm (**Figure 2(b)**). **Figure 2(c)** shows a similar but narrower distribution, with peak intensity around 150-200 nm. **Figure 2(d)** shows a smaller particle size distribution, with peak intensity in the 80-100 nm range, indicating smaller and more uniform particles. **Figure 2(e)** shows a particle size distribution that lies between **Figures 2(b)** and **2(c)**, with peak intensity in the range of 100-150 nm, and **Figure 2(a)** as a control with intensity in the range of 150-300 nm.

Based on this information, we conclude that LNP-mRNA from all lipid mixture concentrations meets nanoparticle size requirements. There is no established ideal size for LNP for drug administration routes. 80-120 nm or ≤ 150 nm are preferred as they can maintain physicochemical integrity and target lymph nodes [39]. Moreover, the size dimensions of viruses and antigens (recombinant proteins) fall within this range, allowing for optimal internalization by APCs. Other studies also indicate that LNPs larger than 100-120 nm have good stability during storage [25,28].

LNP formation using microfluidics is based on the nanoprecipitation method [40] which consists of 4 steps: Supersaturation, nucleation, growth, and stabilization or maturation. Nucleation is a critical stage in the self-assembly of LNPs based on lipid supersaturation concentration. High lipid concentration leads to an increased number of nucleations, thereby enhancing coalescence events and ultimately increasing size [41]. This theory contradicts our findings, as low lipid mixture concentrations of 0.1 and 0.01 mM resulted in larger LNP-mRNA diameters than 1 and 10 mM. We suspect this phenomenon is due to the small amount/ratio of ionized lipids at 0.01 and 0.1 mM lipid mixture concentrations. This leads to low saturation levels and causes aggregation, thus increasing the LNP diameter [42].

Furthermore, the LNP diameter size in dilute lipid solutions forms large particles (up to 800 nm) when low lipid mass fractions are dissolved in high solvent (ethanol) mass fractions. PEG is depleted at the particle interface at low concentrations due to its high solubility in water. This can lead to reduced steric stabilization and accelerated particle growth, resulting in larger diameters and multi-lamellarity [21].

Encapsulation efficiency each lipid mix concentration

Encapsulation efficiency (EE) refers to the percentage of mRNA successfully encapsulated within LNPs, which is crucial for the stability and delivery of mRNA. We used a specific RNA fluorescence dye, RiboGreen, to determine the%EE of each lipid mix

concentration [43]. The RiboGreen assay allows for RNA detection in a fluorescent microplate reader with sensitivity that is 200 times greater than ethidium bromide [44]. The graph shows the encapsulation efficiency (%EE) of LNP-mRNA at various lipid mix concentrations (0.01, 0.1, 1, and 10 mM).

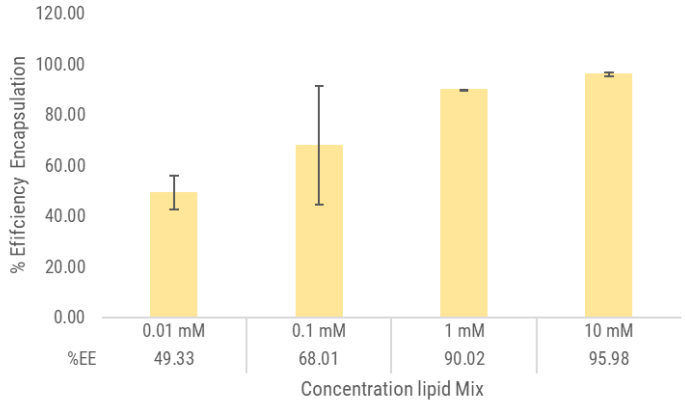

Figure 3 Diagram of encapsulation efficiency for LNP-mRNA at different lipid concentrations.

The data indicate that as the lipid concentration increases, the encapsulation efficiency improves significantly. At lower lipid concentrations (0.01 and 0.1 mM), there is insufficient lipid available to fully encapsulate the mRNA, leading to lower encapsulation efficiencies and more variability. However, at concentrations of 1 and 10 mM, the encapsulation efficiency becomes optimal, with the majority of the mRNA being encapsulated effectively. This finding is similar to the research conducted by Gretchen B. Schober *et al*. [32], where they calculated the%EE at each total lipid concentration of 0.5, 5, and 10 mM. At a concentration of 0.5 mM, the%EE value was lower compared to 5 and 10 mM.

This may be because low concentrations of lipid mix can result in incomplete encapsulation, as there may not be enough lipids to fully surround and protect the mRNA. This can lead to lower encapsulation efficiency, whereas higher lipid concentrations typically provide more lipids to interact with and encapsulate mRNA, potentially increasing the encapsulation efficiency. More lipids form a more stable bilayer around the mRNA, thereby reducing the likelihood of the mRNA escaping from the LNP structure.

This result is consistent with the known relationship between lipid concentration and encapsulation efficiency in nanoparticle formulations. Higher lipid concentrations provide more surface area for mRNA binding and encapsulation, leading to improved stability and delivery potential. However, it is important to balance lipid concentration because too much lipid may lead to increased particle size or other formulation challenges. The findings underscore the importance of optimizing lipid concentration to achieve the highest possible encapsulation efficiency, which is crucial for the effective delivery of mRNA in therapeutic application.

Effect of each molar lipid mix concentration on size and size distribution LNP-mRNA eGFP before and after buffer exchange

Although TFR and FFR affect particle size in microfluidic mixing [23,37,41,45], our experimental results show that the concentration of lipid mixtures influences the size of LNP-mRNA at constant molar lipid ratio, FRR, and TFR parameters. Since the target size of LNP-mRNA is 80-120 nm [25,46], we chose mixed lipid concentrations of 10 and 1 mM. Buffer exchange is an important downstream processing step [47,48]. Mixing LNP-mRNA involves ethanol as a lipid solvent, which can affect the stability of LNPs [49]. The presence of ethanol after the mixing process can lead to an increase in LNP size. Our molecular dynamics simulation results show that the presence of ethanol in the formulation of LNP-mRNA causes aggregation, thereby affecting the particle size of LNPs [50].

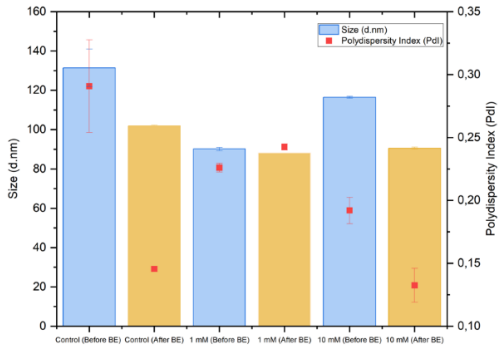

Figure 4 Diagram of LNP-mRNA size before and after buffer exchange.

Buffer exchange was performed using ultrafiltration (UF) with a membrane cut-off of 100 kDa (100 MCWO). On a small laboratory scale, this method accelerates the purification, concentration, and buffer exchange processes [38] compared to using Tangential Flow Filtration (TFF) [47] and dialysis cassettes [48]. Contrary to our prediction, the diameter and PdI of LNP-mRNA decreased in size after buffer exchange with PBS pH 7.4 compared to before the buffer exchange. The average diameter of control LNPs significantly decreased from 137.4 to 101.95 nm after buffer exchange. For 1 mM LNP-mRNA, the average diameter also decreased from 103.1375 to 98.12 nm. Similarly, for 10 mM LNP-mRNA, the average diameter decreased from 118.5 to 90.51 nm. The PdI value of control LNPs significantly decreased from 0.29015 before buffer exchange to 0.1455 after buffer exchange. The PdI value for 1 mM LNP-mRNA in 1 mM PBS buffer slightly increased from 0.226 to 0.2425 after buffer exchange. After buffer exchange, the PdI of 10 mM LNP-mRNA also decreased from 0.192 to 0.1325.

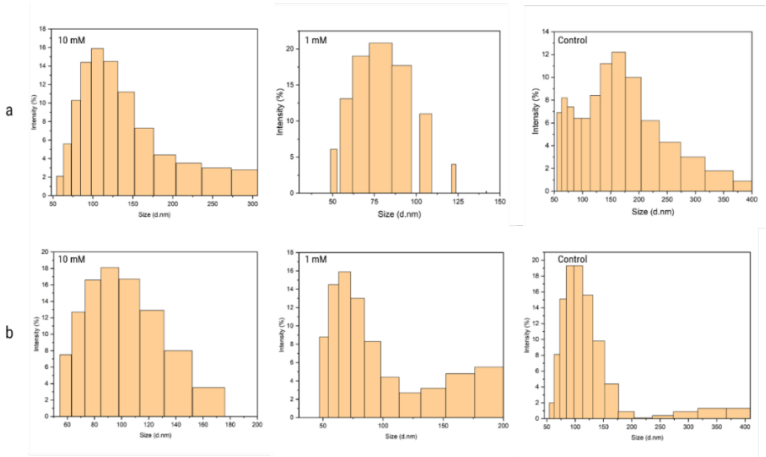

Figure 5 Intensity of distribution size LNP-mRNA: (a) before buffer exchange and (b) after buffer exchange.

The decrease in the average diameter of LNPs and PdI after buffer exchange indicates that the buffer exchange process can lead to particle size reduction and increased homogeneity in particle size distribution. This phenomenon may be related to the redistribution of lipid components or changes in nanoparticle structure. The reduction in LNP-mRNA diameter and the increase in PdI value are likely caused by lipid particles adhering to the surface of LNP-mRNA or forming aggregates that are released due to centrifugal forces and are not retained by the ultrafiltration membrane.

The data on LNP-mRNA size distribution before and after buffer exchange (**Figure 5**) show that the buffer exchange process significantly improves the uniformity and stability of the LNP-mRNA formulation, particularly at higher lipid concentrations (10 and 1 mM). Before buffer exchange, all formulations displayed a broader size distribution, indicating the

presence of particle aggregates or inconsistent particle sizes. This was especially evident in the control samples, where the lack of lipid resulted in the broadest distribution and largest particles.

After buffer exchange, the particle size distribution in all formulations became narrower, with more concentrated peaks. This indicates that buffer exchange helps remove excess components or contaminants that could cause particle aggregation, resulting in more uniform and stable LNP-mRNA particles. The effect is most pronounced in formulations containing lipids, where most particles are now within a tighter size range. Conversely, while the control showed some improvement, it still exhibited a broader distribution compared to lipid formulations, reflecting the role of lipids in the LNP-mRNA formulation.

The effect of each sucrose concentration on size and distribution size LNP-mRNA eGFP

Size is important in drug delivery and targeting, especially for vaccines. The addition of protective substances in the LNP formulation needs to be studied to determine if it affects the size of LNPs. Sucrose is a disaccharide commonly used as a cryoprotectant agent (CPA) [51]. Sucrose can form a glass-like matrix (vitrification) and directly interact with lipids, stabilizing the membrane structure [52]. Sucrose can prevent liposomes from fusing and aggregating, as well as protect the integrity of liposomes from ice crystal formation during freezing and drying processes [53].

Due to its stabilizing properties, we hypothesized that the sucrose concentration would affect the size of LNPs for each lipid formulation concentration. We prepared LNPs with 2 lipid formulation concentrations, each added with 5 and 10% sucrose, while the control LNP group was not supplemented with sucrose. DLS measurements showed that the diameter of LNPs with a 1 mM lipid formulation concentration without sucrose was 88.12 ± 0.1 nm, while for 10 mM, it was 90.51 ± 0.53 nm. After adding sucrose, the particle diameter of LNPs significantly increased with the increase in sucrose concentration for both 1 and 10 mM lipid concentrations (Figure) compared to control LNPs (0% sucrose). The increase in LNP diameter affected the uniformity of the size distribution of LNPs. PdI of the LNPs formulation at a 1 mM lipid concentration showed a decrease in size uniformity; at a 10% sucrose concentration, the PdI value significantly increased from 0.2 to 0.3, whereas at a 10 mM concentration, the size distribution uniformity was maintained with a PdI value of 0.1 across all sucrose concentrations.

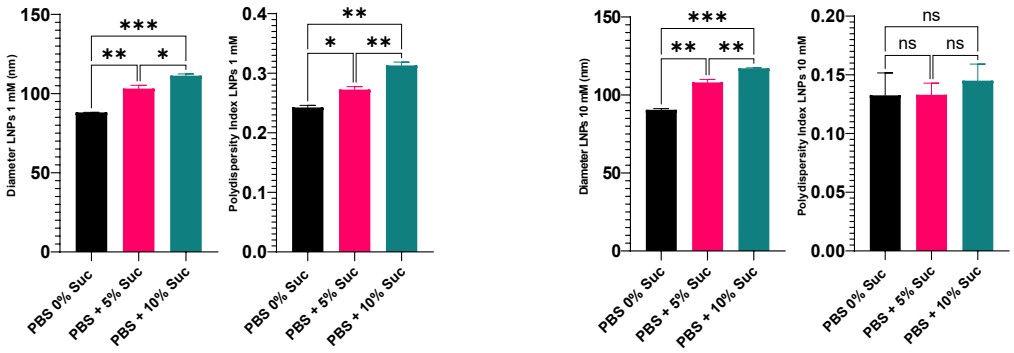

Figure 6 Diagram of the effect of sucrose on particle size for LNP-mRNA with 1 mM (left) and 10 mM (right) lipid concentrations.

The exact mechanism by which sucrose increases the particle size of LNPs is not fully understood. Sucrose is a non-permeable (hydrophobic) type of CPA, which does not penetrate the phospholipid membrane, making it unlikely that the size increase is due to osmotic events. A plausible hypothesis/model regarding how the increase in LNP diameter occurs is the membrane-sugar interaction [54]. It is known that sucrose can form hydrogen bonds (O-H) with the surface of phospholipids (carbonyl and phosphate groups) [55-57] and the methyl group of choline [52]. When added to an LNP suspension, sucrose molecules will occupy the lipid membrane surface, replacing water molecules. This intercalation process causes the membrane heads to

separate, allowing sucrose molecules to enter between the phosphate head groups (hydrophilic) by forming O-H bonds [54,57]. The presence of sucrose between the hydrophilic phospholipid heads causes the membrane to thin and expand, a phenomenon also known as the lateral expansion of the lipid membrane [58]. Research conducted by Roy *et al*. [59] on lipid-membrane interactions using unilamellar vesicles of the phospholipid1,2-dimyristoyl-sn-glycero-3-phosphocholine (DMPC) showed that the presence of sucrose increased the vesicle size as measured by DLS and TEM. In addition to the sugar intercalation process, molecular dynamics studies indicate that sucrose can form more than 10% O-H bonds with phospholipid membranes compared to other disaccharides [60], allowing for size increases due to the accumulation of sucrose on the lipid membrane surface.

Stability size LNP-mRNA eGFP in temperature storage

Previously, we have shown that the diameter and size distribution of LNPs are significantly influenced by the molar concentration of lipids, buffer exchange, and the presence of sucrose as a CPA. We next aimed to evaluate the effect of storage on LNP size stability. Storage with freeze-thaw cycles is an approach that describes the impact of temperature changes during storage and its distribution process. The diameter and size distribution of LNPs were measured weekly and then stored at each storage temperature. A temperature of 2-8°C was used to represent standard medical refrigeration conditions, while –20°C represented the standard freezing temperature of medical freezers, both of which are established by the WHO [61].

Results on the stability of LNP-mRNA formulations over a 4-week period at 2 different freeze-thaw storage temperatures, with various concentrations of sucrose (black, pink, and green bars indicating formulations with 0, 5, and 10% sucrose) and 2 lipid concentrations of 1 mM (left panel) and 10 mM (right panel) are shown in **Figures 7(a)** and **7(b)**, which display the LNP diameter and PdI for storage at 2-8°C. **Figures 8(c)** and **8(d)** show the same metrics for storage at –20°C.

Figures 7(a) and **7(b)** present stability data for LNP-mRNA stored at 2 - 8 °C over a 4-week freeze-thaw period, at 2 lipid concentrations (1 and 10 mM), and various sucrose concentrations (0, 5, and 10%). At 1 mM lipid concentration with 0% sucrose, the LNP diameter increased significantly over time, starting from ~89 nm on day 1 and reaching ~107 nm by week 4. This indicates instability in the LNP-mRNA formulation at 2-8°C without sucrose, likely due to particle aggregation.

With the addition of 5% sucrose, the LNP diameter remained more stable (~113-125 nm), showing moderate increases over time. The presence of sucrose limits the extent of aggregation, but some size increase was still observed by week 4 of the freeze-thaw storage. With 10% sucrose, the LNP diameter remained the most stable, with only slight increases over the 4-week period (~150-181 nm). This indicates that 10% sucrose provides the highest stability, preventing significant particle size growth.

At a lipid concentration of 10 mM, without sucrose (0%), the LNP diameter increased over time similarly to the 1 mM condition, but the changes were less drastic, starting from ~90 nm on day 1 and reaching ~93 nm by week 4. Although particle growth was observed, the higher lipid concentration offered greater inherent stability. With 5 and 10% sucrose, the LNP size remained relatively stable during the storage period (~110-25 nm), with both sucrose concentrations preventing large size fluctuations. However, 10% sucrose demonstrated the best long-term stability.

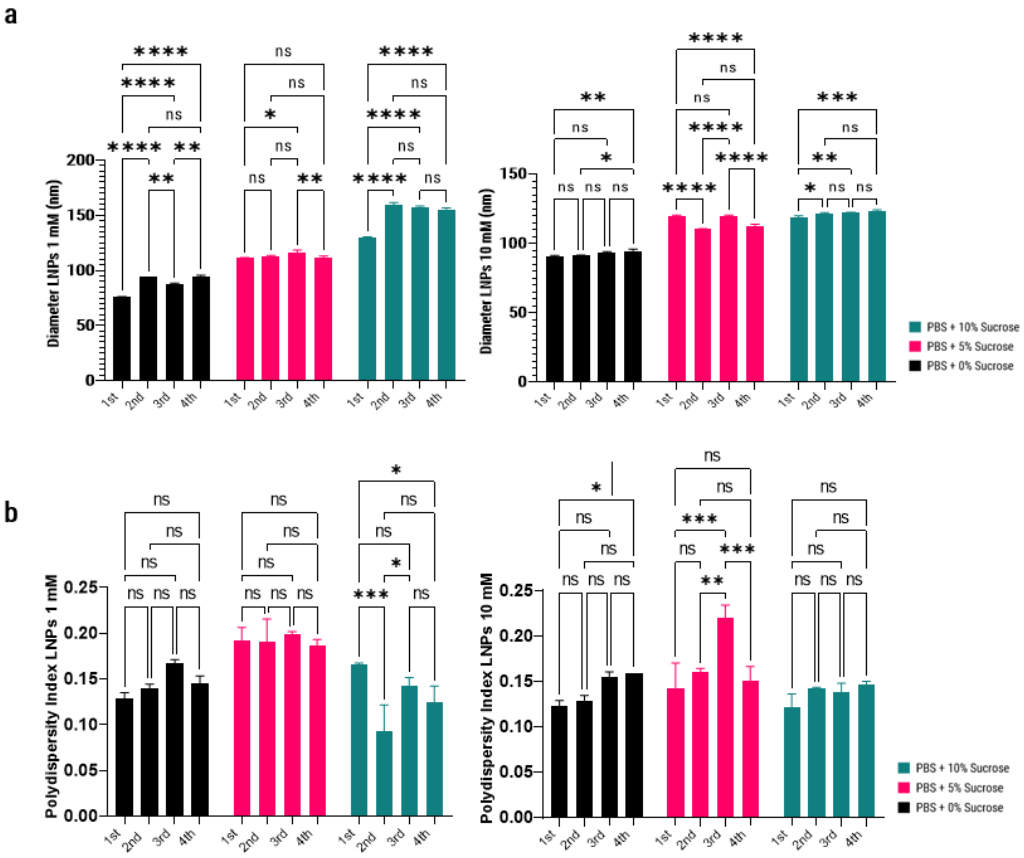

Figure 7 Graph of freeze-thaw storage stability of LNPs at 2-8°C. Diameter of LNPs at 1 and 10 mM concentrations with varying sucrose concentrations of 0, 5, and 10% (a). PdI values of LNPs at 1 and 10 mM concentrations with varying sucrose concentrations of 0, 5, and 10% (b).

The PdI values were relatively high (> 0.2), indicating significant particle size heterogeneity and poor stability at a lipid concentration of 1 mM without sucrose (0%). In contrast, the PdI values decreased with 5 and 10% sucrose, especially with 10% sucrose, which consistently showed lower values (<0.2), indicating better particle size uniformity and overall stability during freeze-thaw storage. At a lipid concentration of 10 mM without sucrose (0%), the PdI remained stable but relatively high (~0.2), indicating size heterogeneity. This suggests that while the particles were less prone to aggregation compared to the 1 mM concentration, there was still room for improvement. The addition of 5 and 10% sucrose in the LNP formulation showed greater particle size uniformity, with a decreasing PdI value, especially with 10% sucrose. The 10 mM lipid concentration was inherently more stable, and the addition of sucrose further enhanced its stability.

Regarding LNP diameter (**Figure 8(C)**), at a 1 mM lipid concentration in the formulation without sucrose (0%), there was significant variability over time, with an initially large diameter (~200 nm) that decreased over time. This indicates that the LNP-mRNA formulation without sucrose was less stable at –20°C, leading to fluctuations in particle size. With the addition of 5% sucrose, the diameter remained stable between ~100-130 nm, suggesting that sucrose helped maintain LNP size over time. With the addition of 10% sucrose, the LNP showed better stability, with consistently smaller sizes (~150 nm) during the 1st 2 weeks, although particle size increased during the 3rd and 4th weeks.

At a lipid concentration of 10 mM, LNPs without sucrose showed similar size variation patterns over time. However, the changes were less pronounced compared to the 1 mM condition, with particle sizes remaining more stable (~100-110 nm). LNPs with 5 and 10% sucrose demonstrated stable sizes over time (~130 nm), indicating that even at higher lipid concentrations, sucrose effectively maintained particle size stability at –20°C.

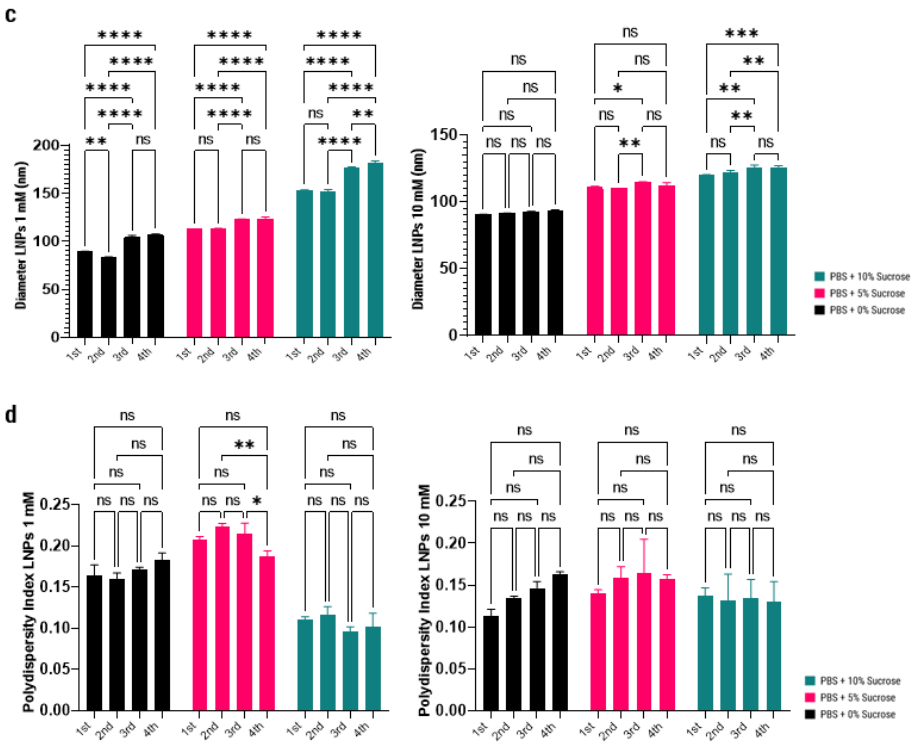

Figure 8 Diagram of freeze-thaw storage stability of LNPs at –20°C. Diameter of LNPs at 1 and 10 mM concentrations with varying sucrose concentrations of 0, 5, and 10% (c). PdI values of LNPs at 1 and 10 mM concentrations with varying sucrose concentrations of 0, 5, and 10% (d).

At a lipid concentration of 1 mM, LNPs without sucrose exhibited a relatively high PdI (> 0.2), compared to a 5% sucrose concentration, which showed greater particle size heterogeneity. This reflects poor stability, with nanoparticles potentially undergoing aggregation or degradation. The addition of 10% sucrose significantly reduced the PdI to below 0.2, with 10% sucrose displaying the most consistent particle size uniformity, helping to maintain homogeneity and prevent aggregation in LNP-mRNA formulations. At a lipid concentration of 10 mM, the PdI remained below 0.2, indicating that LNPs at this lipid concentration were more stable, even without sucrose. However, the 5 and 10% sucrose formulations still showed slightly better particle uniformity, with lower and more consistent PdI values.

Storage at –20°C in liquid conditions was superior to storage at 2-8°C in maintaining the stability of the LNP-mRNA formulations. LNPs without sucrose stored at –20°C tended to be more stable in terms of size and PdI than those stored at 2-8°C. However, the addition of sucrose, especially at 10%, significantly enhanced particle stability and size uniformity, regardless of lipid concentration or storage temperature. Our findings are consistent with the research conducted by Kim *et al.* [62], which showed that a 10% sucrose concentration can maintain the physical stability of RNA (repRNA) loaded in LNPs at –20°C. Other studies also mention that the addition of 10% sucrose improves stability during storage [63,64]. Sucrose acts as a CPA preventing clumping and preserving particle size and uniformity during freeze-thaw storage, especially at lower temperatures (–20°C). The mechanism of sucrose as a CPA is not precisely known, but there is a strong hypothesis that sucrose interferes with water molecule interactions by forming water-sucrose hydrogen bonds, there by inhibiting the formation of ice crystals [65]. Sucrose is a CPA that can increase the glass transition temperature (Tg), at which molecular movement is reduced, enhancing resistance to the crystallization process [66]. The combination of 10 mM lipid concentration and 10% sucrose provided the best overall stability for LNP-mRNA formulations stored at any temperature, but storage at –20°C was ideal for long-term preservation of these formulations.

Overall, the results indicate that the freeze-thaw storage process affects LNP stability, and sucrose can modulate this effect, although not uniformly across different lipid concentrations. These findings align with the understanding that LNP formulations require careful optimization of cryoprotectants to ensure size and distribution stability, which is critical for maintaining the efficacy and safety of therapeutic agents delivered [67]. A lower PdI indicates a narrow size distribution, which is desirable for consistent drug delivery performance. The PdI values of all tested LNPs increased over several weeks, indicating an increase in particle size distribution due to freeze-thaw stress. However, LNPs with 10 mM lipid and 10% sucrose across all storage temperatures showed no significant differences in PdI values, suggesting a more uniform particle size distribution that could result in more consistent biodistribution and clinical efficacy.

Conclusions

This study investigated the effects of molar concentration of lipid mixtures and sucrose addition on the size and stability of LNPs encapsulating mRNA, exploring their potential implications for vaccine delivery. Our results affirm the pivotal role of lipid concentration in defining both the size and encapsulation efficiency of LNPs. Higher lipid concentrations demonstrated improved encapsulation efficiencies and yielded nanoparticles within the optimal size range of 80-120 nm, ideal for immune cell recognition and subsequent lymphatic system trafficking. Microfluidic mixing, a critical process in the formulation of LNPs, enabled the precise control of nanoparticle size and distribution, achieving monodispersity as indicated by PdI values below 0.3. This size precision is crucial for consistent biodistribution and immune response, a key factor in vaccine efficacy. Furthermore, the addition of sucrose as a cryoprotectant significantly influenced the physical stability of LNPs. While sucrose enhanced size stability during freeze-thaw cycles, it also affected the size distribution depending on its concentration. This highlights the necessity of optimizing sucrose levels to balance cryoprotection with the maintenance of desired nanoparticle size and distribution, especially under various storage conditions. Lastly, the study underscored the importance of storage conditions, with LNPs showing distinct stability profiles at 2-8°C and –20°C. Sucrose proved to be beneficial in preserving LNPs' structural integrity and size uniformity during storage, with a notable enhancement in stability at lower temperatures. Collectively, these findings contribute to the ongoing development of mRNA vaccine formulations, suggesting that a nuanced understanding of lipid and sucrose concentrations is essential for optimizing LNP systems. These insights pave the way for enhancing the practicality and effectiveness of mRNA-based therapeutics, potentially improving the outcomes of vaccination programs worldwide.

Acknowledgements

We acknowledge BRIN and LPDP for the RIIM Grant, grant number 44/IV/KS/06/2022, and to PT. Bio Farma Indonesia for their valuable support and for providing all the research facilities.

References

[1] A Saleh, S Qamar, A Tekin, R Singh and R Kashyap. Vaccine development throughout history. *Cureus* 2021; **13(7)**, e16635.

[2] A Fortner and D Schumacher. First COVID-19 vaccines receiving the US FDA and EMA emergency use authorization. *Discoveries* 2021; **9(1)**, e122.

[3] GS Laurini, N Montanaro, M Broccoli, G Bonaldo and D Motola. Real-life safety profile of mRNA vaccines for COVID-19: An analysis of VAERS database. *Vaccine* 2023; **41(18)**, 2879-2886.

[4] M Schlich, R Palomba, G Costabile, S Mizrahy, M Pannuzzo, D Peer and P Decuzzi. Cytosolic delivery of nucleic acids: The case of ionizable lipid nanoparticles. *Bioengineering & Translational Medicine* 2021; **6(2)**, e10213.

[5] MCP Mendonça, A Kont, PS Kowalski and CM O'Driscoll. Design of lipid-based nanoparticles for delivery of therapeutic nucleic acids. *Drug Discovery Today* 2023; **28(3)**, 103505.

[6] BZ Igyártó and Z Qin. The mRNA-LNP vaccines - the good, the bad and the ugly? *Frontiers in Immunology* 2024; **15**, 1336906.

[7] M Sedic, JJ Senn, A Lynn, M Laska, M Smith, SJ Platz, J Bolen, S Hoge, A Bulychev, E Jacquinet, V Bartlett and PF Smith. Safety evaluation of lipid nanoparticle-formulated modified mRNA in the

Sprague-Dawley rat and cynomolgus monkey. *Veterinary Pathology* 2018; **55(2)**, 341-354.

[8] M Yang, Z Zhang, P Jin, K Jiang, Y Xu, F Pan, K Tian, Z Yuan, XE Liu, J Fu, B Wang, H Yan, C Zhan and Z Zhang. Effects of PEG antibodies on *in vivo* performance of LNP-mRNA vaccines. *International Journal of Pharmaceutics* 2024; **650**, 123695.

[9] R Tenchov, R Bird, AE Curtze and Q Zhou. Lipid nanoparticles - From liposomes to mRNA vaccine delivery, a landscape of research diversity and advancement. *ACS Nano* 2021; **15(11)**, 16982-17015.

[10] E Álvarez-Benedicto, L Farbiak, MM Ramírez, X Wang, LT Johnson, O Mian, ED Guerrero and DJ Siegwart. Optimization of phospholipid chemistry for improved lipid nanoparticle (LNP) delivery of messenger RNA (mRNA). *Biomaterials Science* 2022; **10(2)**, 549-559.

[11] CH Albertsen, JA Kulkarni, D Witzigmann, M Lind, K Petersson and JB Simonsen. The role of lipid components in lipid nanoparticles for vaccines and gene therapy. *Advanced Drug Delivery Reviews* 2022; **188**, 114416.

[12] HN Jung, SY Lee, S Lee, H Youn and HJ Im. Lipid nanoparticles for delivery of RNA therapeutics: Current status and the role of *in vivo* imaging. *Theranostics* 2022; **12(17)**, 7509-7531.

[13] M Tang, A Sagawa, N Inoue, S Torii, K Tomita and Y Hattori. Efficient mRNA delivery with mRNA lipoplexes prepared using a modified ethanol injection method. *Pharmaceutics* 2023; **15(4)**, 1141.

[14] C Zhang, Y Ma, J Zhang, JCT Kuo, Z Zhang, H Xie, J Zhu and T Liu. Modification of lipid-based nanoparticles: An efficient delivery system for nucleic acid-based immunotherapy. *Molecules* 2022; **27**, 1943.

[15] AD Bangham, MM Standish and JC Watkins. Diffusion of univalent ions across the lamellae of swollen phospholipids. *Journal of Molecular Biology* 1965; **13(1)**, 238-252.

[16] RE McKenzie, JJ Minnell, M Ganley, GF Painter and SL Draper. mRNA synthesis and encapsulation in ionizable lipid nanoparticles. *Current Protocols* 2023; **3(9)**, e898.

[17] CJM Rivas, M Tarhini, W Badri, K Miladi, H Greige-Gerges, QA Nazari, SAG Rodríguez, RÁ Román, H Fessi and A Elaissari. Nanoprecipitation process: From encapsulation to drug delivery. *International Journal of Pharmaceutics* 2017; **532(1)**, 66-81.

[18] BG Carvalho, BT Ceccato, M Michelon, SW Han and LGDL Torre. Advanced microfluidic technologies for lipid nano-microsystems from synthesis to biological application. *Pharmaceutics* 2022; **14(1)**, 141.

[19] S Salatin, J Barar, M Barzegar-Jalali, K Adibkia, F Kiafar and M Jelvehgari. Development of a nanoprecipitation method for the entrapment of a very water soluble drug into Eudragit RL nanoparticles. *Research in Pharmaceutical Sciences* 2017; **12(1)**, 1-14.

[20] M Maeki, T Saito, Y Sato, T Yasui, N Kaji, A Ishida, H Tani, Y Baba, H Harashima and M Tokeshi. A strategy for synthesis of lipid nanoparticles using microfluidic devices with a mixer structure. *RSC Advances* 2015; **5(57)**, 46181-46185.

[21] J Nguyen, CL Walsh, JPM Motion, EK Perttu and F Szoka. Controlled nucleation of lipid nanoparticles. *Pharmaceutical Research* 2012; **29(8)**, 2236-2248.

[22] KJ Wu, ECM Tse, C Shang and Z Guo. Nucleation and growth in solution synthesis of nanostructures - From fundamentals to advanced applications. *Progress in Materials Science* 2022; **123**, 100821.

[23] M Maeki, S Uno, A Niwa, Y Okada and M Tokeshi. Microfluidic technologies and devices for lipid nanoparticle-based RNA delivery. *Journal of Controlled Release* 2022; **344**, 80-96.

[24] AD Stroock, SKW Dertinger, A Ajdari, I Mezić, HA Stone and GM Whitesides. Chaotic mixer for microchannels. *Science* 2002; **295(5555)**, 647-651.

[25] KJ Hassett, J Higgins, A Woods, B Levy, Y Xia, CJ Hsiao, E Acosta, Ö Almarsson, MJ Moore and LA Brito. Impact of lipid nanoparticle size on mRNA vaccine immunogenicity. *Journal of Controlled Release* 2021; **335**, 237-246.

[26] T Nakamura, M Kawai, Y Sato, M Maeki, M Tokeshi and H Harashima. The effect of size and charge of lipid nanoparticles prepared by

microfluidic mixing on their lymph node transitivity and distribution. *Molecular Pharmaceutics* 2020; **17(3)**, 944-953.

[27] M Dhayalan, W Wang, SUM Riyaz, RA Dinesh, J Shanmugam, SS Irudayaraj, A Stalin, J Giri, S Mallik and R Hu. Advances in functional lipid nanoparticles: From drug delivery platforms to clinical applications. *3 Biotech* 2024; **14(2)**, 57.

[28] MF Bachmann and GT Jennings. Vaccine delivery: A matter of size, geometry, kinetics and molecular patterns. *Nature Reviews Immunology* 2010; **10**, 787-796.

[29] A Ji, M Xu, Y Pan, L Diao, L Ma, L Qian, J Cheng and M Liu. Lipid microparticles show similar efficacy with lipid nanoparticles in delivering mRNA and preventing cancer. *Pharmaceutical Research* 2023; **40(1)**, 265-279.

[30] M Kovacsovics-Bankowski, K Clark, B Benacerraf and KL Rock. Efficient major histocompatibility complex class I presentation of exogenous antigen upon phagocytosis by macrophages. *Proceedings of the National Academy Sciences of the United States of America* 1993; **90(11)**, 4942-4946.

[31] H Pflicke and M Sixt. Preformed portals facilitate dendritic cell entry into afferent lymphatic vessels. *The Journal of Experimental Medicine* 2009; **206(13)**, 2925-2935.

[32] GB Schober, S Story and DP Arya. A careful look at lipid nanoparticle characterization: Analysis of benchmark formulations for encapsulation of RNA cargo size gradient. *Scientific Reports* 2024; **14(1)**, 2403.

[33] A Lamoot, J Lammens, ED Lombaerde, Z Zhong, M Gontsarik, Y Chen, TRMD Beer and BGD Geest. Successful batch and continuous lyophilization of mRNA LNP formulations depend on cryoprotectants and ionizable lipids. *Biomaterials Science* 2023; **11(12)**, 4327-4334.

[34] P Zhao, X Hou, J Yan, S Du, Y Xue, W Li, G Xiang and Y Dong. Long-term storage of lipid-like nanoparticles for mRNA delivery. *Bioactive Materials* 2020; **5(2)**, 358-363.

[35] A Akinc, MA Maier, M Manoharan, K Fitzgerald, M Jayaraman, S Barros, S Ansell, X Du, MJ Hope, TD Madden, BL Mui, SC Semple, YK Tam, M Ciufolini, D Witzigmann, JA Kulkarni, RVD Meel and PR Cullis. The Onpattro story and the clinical translation of nanomedicines containing nucleic acid-based drugs. *Nature Nanotechnology* 2019; **14(12)**, 1084-1087.

[36] C Walsh, K Ou, NM Belliveau, TJ Leaver, AW Wild, J Huft, PJ Lin, S Chen, AK Leung, JB Lee, CL Hansen, RJ Taylor, EC Ramsay and PR Cullis. Microfluidic-based manufacture of siRNA-lipid nanoparticles for therapeutic applications. *Methods in Molecular Biology* 2014; **1141**, 109-120.

[37] NM Belliveau, J Huft, PJC Lin, S Chen, AKK Leung, TJ Leaver, AW Wild, JB Lee, RJ Taylor, YK Tam, CL Hansen and PR Cullis. Microfluidic synthesis of highly potent limit-size lipid nanoparticles for *in vivo* delivery of siRNA. *Molecular Therapy Nucleic Acids* 2012; **1**, e37.

[38] CM Bailey-Hytholt, P Ghosh, J Dugas, IE Zarraga and A Bandekar. Formulating and characterizing lipid nanoparticles for gene delivery using a microfluidic mixing platform. *Journal of Visualized Experiments* 2021. https://doi.org/10.3791/62226.

[39] R Shi, X Liu, Y Wang, M Pan, S Wang, L Shi and B Ni. Long-term stability and immunogenicity of lipid nanoparticle COVID-19 mRNA vaccine is affected by particle size. *Human Vaccines & Immunotherapeutics* 2024; **20**, 2342592.

[40] M Mehta, TA Bui, X Yang, Y Aksoy, EM Goldys and W Deng. Lipid-based nanoparticles for drug/gene delivery: An overview of the production techniques and difficulties encountered in their industrial development. *ACS Materials Au* 2023; **3(6)**, 600-619.

[41] M Maeki, Y Fujishima, Y Sato, T Yasui, N Kaji, A Ishida, H Tani, Y Baba, H Harashima and M Tokeshi. Understanding the formation mechanism of lipid nanoparticles in microfluidic devices with chaotic micromixers. *PLoS One* 2017; **12(11)**, e0187962.

[42] SM D'Addio and RK Prud'Homme. Controlling drug nanoparticle formation by rapid precipitation. *Advanced Drug Delivery Reviews* 2011; **63(6)**, 417-426.

[43] JG Hashimoto, AS Beadles-Bohling and KM Wiren. Comparison of RiboGreen® and 18S rRNA quantitation for normalizing real-time RT-

PCR expression analysis. *Biotechniques* 2004; **36(1)**, 54-60.

[44] LJ Jones, ST Yue, CY Cheung and VL Singer. RNA quantitation by fluorescence-based solution assay: RiboGreen reagent characterization. *Analytical Biochemistry* 1998; **265(2)**, 368-374.

[45] CB Roces, G Lou, N Jain, S Abraham, A Thomas, GW Halbert and Y Perrie. Manufacturing considerations for the development of lipid nanoparticles using microfluidics. *Pharmaceutics* 2020; **12(11)**, 1095.

[46] EVL Grgacic and DA Anderson. Virus-like particles: Passport to immune recognition. *Methods* 2006; **40(1)**, 60-65.

[47] R Mihaila, S Chang, AT Wei, ZY Hu, D Ruhela, TR Shadel, S Duenwald, E Payson, JJ Cunningham, N Kuklin and DJ Mathre. Lipid nanoparticle purification by Spin Centrifugation-Dialysis (SCD): A facile and high-throughput approach for small scale preparation of siRNA-lipid complexes. *International Journal of Pharmaceutics* 2011; **420(1)**, 118-121.

[48] R Vargas, M Romero, T Berasategui, DA Narváez-Narváez, P Ramirez, A Nardi-Ricart, E García-Montoya, P Pérez-Lozano, JM Suñe-Negre, C Moreno-Castro, C Hernández-Munain, C Suñe and M Suñe-Pou. Dialysis is a key factor modulating interactions between critical process parameters during the microfluidic preparation of lipid nanoparticles. *Colloid and Interface Science Communications* 2023; **54**, 100709.

[49] L Schoenmaker, D Witzigmann, JA Kulkarni, R Verbeke, G Kersten, W Jiskoot and DJA Crommelin. mRNA-lipid nanoparticle COVID-19 vaccines: Structure and stability. *International Journal of Pharmaceutics* 2021; **601**, 120586.

[50] A Hardianto, ZS Muscifa, W Widayat, M Yusuf and T Subroto. The effect of ethanol on lipid nanoparticle stabilization from a molecular dynamics simulation perspective. *Molecules* 2023; **28(12)**, 4836.

[51] GF Boafo, KT Magar, MD Ekpo, W Qian, S Tan and C Chen. The role of cryoprotective agents in liposome stabilization and preservation. *International Journal of Molecular Sciences* 2022; **23(20)**, 12487.

[52] C Cacela and DK Hincha. Low amounts of sucrose are sufficient to depress the phase transition temperature of dry phosphatidylcholine, but not for lyoprotection of liposomes. *Biophysical Journal* 2006; **90(8)**, 2831.

[53] D Guimarães, J Noro, C Silva, A Cavaco-Paulo and E Nogueira. Protective effect of saccharides on freeze-dried liposomes encapsulating drugs. *Frontiers in Bioengineering and Biotechnology* 2019; **7**, 424.

[54] HD Andersen, C Wang, L Arleth, GH Peters and P Westh. Reconciliation of opposing views on membrane-sugar interactions. *Proceedings of the National Academy of Sciences of the United States of America* 2011; **108(5)**, 1874-1878.

[55] JH Crowe, LM Crowe, JF Carpenter, AS Rudolph, CA Wistrom, BJ Spargo and TJ Anchordoguy. Interactions of sugars with membranes. *Biochimica et Biophysica Acta* 1988; **947(2)**, 367-384.

[56] JH Crowe, FA Hoekstra, KHN Nguyen and LM Crowe. Is vitrification involved in depression of the phase transition temperature in dry phospholipids? *Biochimica et Biophysica Acta* 1996; **1280(2)**, 187-196.

[57] IJ Vereyken, V Chupin, RA Demel, SC Smeekens and BD Kruijff. Fructans insert between the headgroups of phospholipids. *Biochimica et Biophysica Acta* 2001; **1510(1-2)**, 307-320.

[58] A Dhaliwal, A Khondker, R Alsop and MC Rheinstädter. Glucose can protect membranes against dehydration damage by inducing a glassy membrane state at low hydrations. *Membranes* 2019; **9(1)**, 15.

[59] A Roy, R Dutta, N Kundu, D Banik and N Sarkar. A comparative study of the influence of sugars sucrose, trehalose, and maltose on the hydration and diffusion of DMPC lipid bilayer at complete hydration: Investigation of structural and spectroscopic aspect of lipid-sugar interaction. *Langmuir* 2016; **32(20)**, 5124-5134.

[60] GVD Bogaart, N Hermans, V Krasnikov, AHD Vries and B Poolman. On the decrease in lateral mobility of phospholipids by sugars. *Biophysical Journal* 2007; **92(5)**, 1598-1605.

[61] Ü Kartoglu, NK Özgüler, LJ Wolfson and W Kurzatkowski. Validation of the shake test for

detecting freeze damage to adsorbed vaccines. *Bulletin of the World Health Organization* 2010; **88(8)**, 624-631.

[62] B Kim, RR Hosn, T Remba, D Yun, N Li, W Abraham, MB Melo, M Cortes, B Li, Y Zhang, Y Dong and DJ Irvine. Optimization of storage conditions for lipid nanoparticle-formulated self-replicating RNA vaccines. *Journal of Controlled Release* 2023; **353**, 241-253.

[63] SC Rumsey, NF Galeano, Y Arad and RJ Deckelbaum. Cryopreservation with sucrose maintains normal physical and biological properties of human plasma low density lipoproteins. *Journal of Lipid Research* 1992; **33(10)**, 1551-1561.

[64] G Yu, R Li and A Hubel. Interfacial interactions of sucrose during cryopreservation detected by Raman spectroscopy. *Langmuir* 2019; **35(23)**, 7388-7395.

[65] MJGW Roozen and MA Hemminga. Molecular motion in sucrose-water mixtures in the liquid and glassy state as studied by spin probe ESR. *Journal of Physical Chemistry* 1990; **94(18)**, 7326-7329.

[66] WQ Sun, AC Leopold, LM Crowe and JH Crowe. Stability of dry liposomes in sugar glasses. *Biophysical Journal* 1996; **70(4)**, 1769-1776.

[67] G Anderluzzi, G Lou, S Woods, ST Schmidt, S Gallorini, M Brazzoli, R Johnson, CW Roberts, DT O'Hagan, BC Baudner and Y Perrie. The role of nanoparticle format and route of administration on self-amplifying mRNA vaccine potency. *Journal of Controlled Release* 2022; **342**, 388-399.